Engineering Structures 168 (2018) 23–34

Contents lists available at ScienceDirect

Engineering Structures

journal homepage: www.elsevier.com/locate/engstruct

# Buckling analysis and design proposal for 2-side supported double Insulated Glass Units (IGUs) in compression

Chiara Bedon*, Claudio Amadio

*University of Trieste, Department of Engineering and Architecture, Piazzale Europa 1, 34127 Trieste, Italy*

ARTICLE INFO

*Keywords:*
Structural glass
Insulated Glass Units (IGUs)
Load sharing effects
Buckling
Global imperfections
Temperature gradients
Standardized design curves
Analytical methods
Finite element numerical modelling

ABSTRACT

Due to mainly thermal and energy potentials, Insulated Glass Units (IGUs) are largely used in modern buildings to realize curtain walls and enclosures. The typical IGU consists of two glass layers, either monolithic and/or laminated, joined together by enclosing an hermetically-sealed air (or gas) cavity between them. There, maximum stresses and deformations derive from external pressures (wind loads, etc.) or environmental/climatic loads (temperature variations, etc.). While the common IGU application involves 4-side continuous supports, novel restraint configurations are increasingly used in practice (i.e. 2-side supports, point-fixings, etc.), hence resulting in additional loading scenarios that could compromise the integrity of these systems. In this paper, following earlier research contributions, a standardized buckling approach in use for structural glass elements mainly compressed or under combined compression/bending is assessed, for the specific case of IGUs with 2-side continuous supports. Analytical and Finite Element (FE) numerical studies are reported, giving evidence of their actual performance and buckling resistance, including parametric analyses and comparisons towards simplified design formulations for both external and internal pressures.

## 1. Introduction

The use of glass components in constructions as an efficient load bearing solution is relatively recent, compared to consolidated structural applications of timber, steel, concrete or masonry in buildings. Major positive arguments of glass facades are related to the thermal, energy, light and aesthetic advantages. In terms of structural performances, however, the low tensile resistance, the high slenderness and flexibility of glass components represent the major issues in design, since stress peaks and large deformations should be prevented via appropriate *fail-safe* criteria (i.e. [1,2]). Special care should be spent especially to avoid possible buckling phenomena and premature losses of stability.

In this research study, extended investigations are focused on the buckling analysis of Insulated Glass Units (IGUs), being of large use in curtain walls and envelopes in buildings [3,4]. In the current design practice, the conventional IGU application includes 4-side supported glass panels, via metal frames acting as continuous bracing systems (see for example Fig. 1(a)). Novel solutions aimed to replace the metal framing members with thermo-mechanical efficient systems are under investigation [5–7]. For design purposes, special care should be spent especially for innovative boundary conditions (2-side supports, mechanical point-fixings, etc.), being increasingly used in buildings for IGUs spanning from floor-to-floor.

In this paper, double IGUs composed of two glass panels with a cavity gap interposed, restrained via linear top/bottom supports and under a combination of in-plane compressive loads and orthogonal pressures, are explored. There, linear top/bottom continuous supports can take the form of metal brackets preventing lateral displacements/rotations and gaskets/spacers able to avoid local damage and stress peaks in glass, see Fig. 1(c) and (d). Alternative solutions can involve aluminium or steel U-channel and “shoe” profiles, with equivalent effects and designed to withstand reaction forces transferred from the glass panels [2,8]. Non-structural sealant joints along the vertical edges ensure the visual continuity to glazing enclosures, but result in a rather vulnerable boundary condition to properly assess (see also [9,10]). Major outcomes are derived in this research study from advanced Finite Element (FE) numerical simulations [11] and past analytical models for the buckling performance assessment of single glass members under various loading/boundary conditions (see [12–15]).

Given the actual geometrical features, material properties and typical high slenderness ratios of glazing systems, the effects of design loads should be checked with respect to possible buckling phenomena. So far, research efforts have been spent for stability losses in compressed structural glass members [16–23]. This is not the case of IGUs, where the actual load bearing performance is strictly related to the

* Corresponding author.
*E-mail address:* chiara.bedon@dia.units.it (C. Bedon).

https://doi.org/10.1016/j.engstruct.2018.04.055
Received 28 December 2017; Received in revised form 13 April 2018; Accepted 16 April 2018

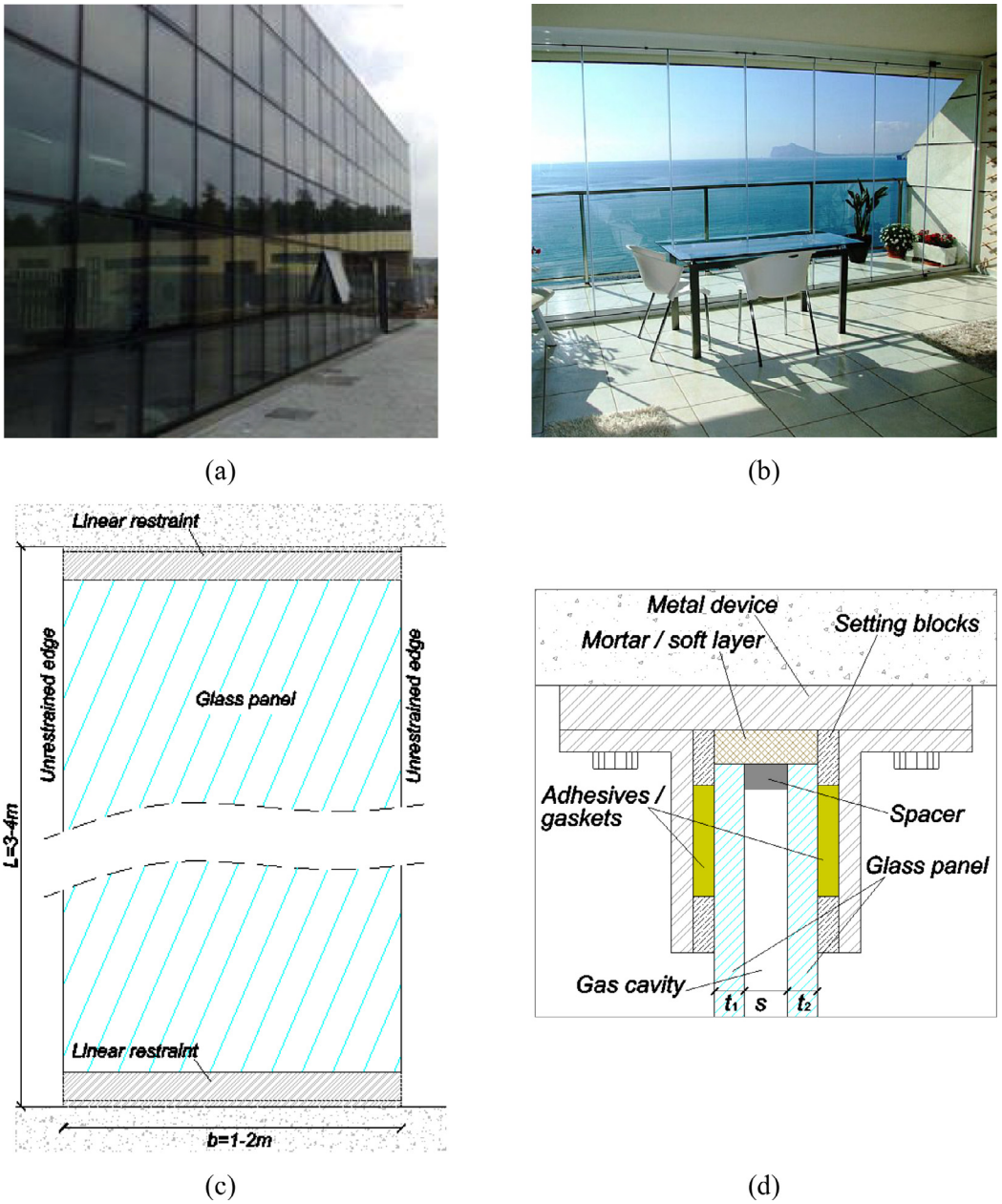


**Fig. 1.** IGUs in enclosures and curtain walls: examples of (a) 4-side or (b) 2-side supported panels, with (c) reference mechanical system and (d) typical restraint detail (cross-section).

additional effect of combined (shared) loads, both in presence of external (wind, crowd, maintenance, etc.) and internal (environmental loads inclusive of temperature, pressure and altitude variations) design actions.

Moreover, the structural role of linear spacers along the glass panels edges (see Fig. 2) represents a further aspect still requiring investigations. There, a flexible silicon joint and a mostly rigid bar (composed of metal or fiberglass thin profiles [3]) are in fact aimed only to keep fix the position of glass layers. When the glass panels are obtained from laminated glass (LG) sections, finally, the effects of flexible interlayer foils with mechanical properties depending on time loading/temperature conditions should be also taken into account (see for example [1,2,15]).

In this paper, aiming to provide useful design recommendations for 2-side supported, compressed IGUs according to Fig. 1(c), buckling design considerations are first briefly summarized (Section 2), giving evidence of standardized methods in use for (independent) single glass members. A refined FE modelling approach implemented in ABAQUS [11] is presented (Section 3), to explore the typical performance of IGUs under in-plane compressive loads. Several geometrical configurations are considered, by accounting for the gas cavity effects and giving evidence of the actual 'coupled' response of glass layers. Based on preliminary FE observations, simplified analytical expressions are also proposed in Section 3, highlighting the limited load bearing capacity of 2-side restrained IGUs. Section 4 focuses then on the combined compressive/bending response of the same IGUs, as it is in most of practical configurations. Simplified analytical formulations for a possible buckling design standardization are finally assessed and discussed towards FE predictions.

## 2. General buckling design considerations and existing analytical methods

While most of IGU studies have been focused on thermal, durability

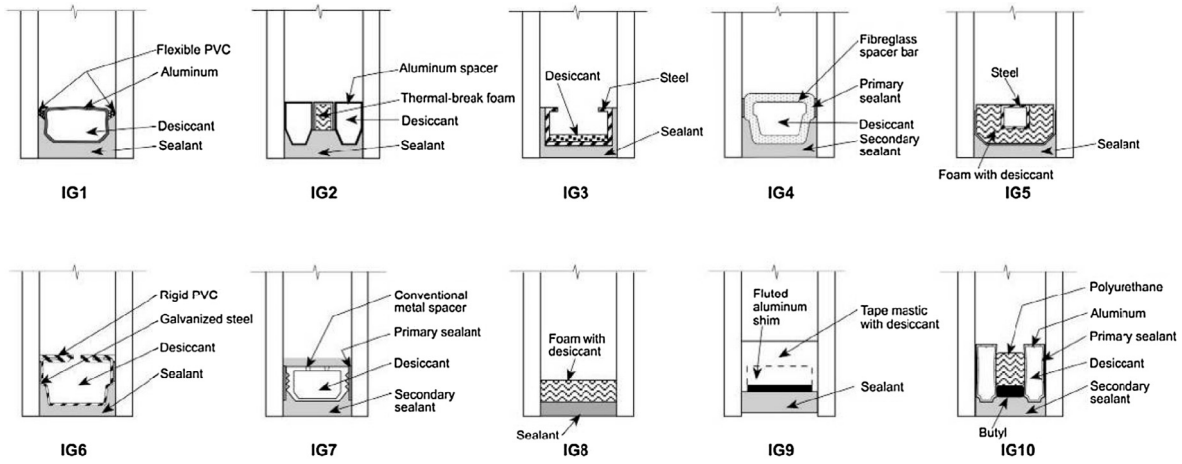


**Fig. 2.** Examples of spacers in use for double IGUs (schematic drawings reported from [3]).

and sound insulation aspects ([3,4,24–31], etc.) or facade applications ([32–36], etc.), limited research efforts have been dedicated to the structural performance of IGUs [37–42], including preliminary load bearing assessment of spacers [43,44]. In most of the cases, 4-side continuous supports have been only considered (Fig. 1(a)), giving evidence of the so-called *load sharing* phenomena under out-of-plane deformations. There, the actual flexibility and resistance of spacers (Fig. 2) has been generally disregarded, assuming an ideal, linear rigid connection along the panels' edges ([15,45,46], etc.). Design uncertainties increase – requiring full-scale testing and/or advanced FE numerical models – for IGUs under different boundary/loading conditions [47,48], including impact and/or explosive events [49–51].

The buckling performance of 2-side supported IGUs as composite structural systems represents an open issue for design, due to the increasingly use of novel boundary configurations. Critical conditions for fail-safe design purposes, see Fig. 1(b)–(d), could derive from a combination of multiple aspects, including design actions (internal and/or external), typical high slendernesses, limited glass thicknesses with high size-to-thickness ratios, limited tensile resistance of glass [52], global initial imperfections, lack of robust restraints, etc. As in the general case of single structural glass elements [12,13,15], appropriate verification criteria are hence required.

### 2.1. Glass members under in-plane compression

According to the Limit State design approach for structural members in compression [1,2], the buckling collapse of glass columns should be prevented by simultaneously limiting maximum tensile stresses $\sigma_{max}$ and out-of-plane deflections $w_{max}$ due to the imposed loads $N_{Ed}$

From a practical point of view, it was shown in [13] that standardized buckling curves can be used for single 'independent' glass members, to accomplish for stress, deflection and design action requirements via a suitable and robust tool for design [15]. Given a pinned glass column, its design buckling resistance can be expressed as (with $A = t \times b$ the cross-sectional area, $\sigma_R$ the nominal tensile resistance and $\gamma_{M1}$ a partial safety factor):

$$N_{b,Rd} = \chi \cdot \frac{A\sigma_R}{\gamma_{M1}} \tag{1}$$

where the buckling reduction factor $\chi$ for the fundamental buckling mode is given by:

$$\chi = \frac{1}{\Phi + \sqrt{\Phi^2 - \overline{\lambda}^2}} \quad (\chi \leqslant 1), \tag{2}$$

with:

$$\Phi = 0.5 \cdot [1 + \alpha_{imp}(\overline{\lambda} - \alpha_0) + \overline{\lambda}^2] \tag{3}$$

and:

$$\overline{\lambda} = \sqrt{\frac{A\sigma_R}{N_{cr}^{(E)}}}, \tag{4}$$

the shape function and the normalized slenderness respectively, while $N_{cr}^{(E)}$ is the conventional Euler's critical load.

In Eq. (3), the imperfection factors $\alpha_{imp} = 0.6$ and $\alpha_0 = 0.71$ can be used for initial geometrical imperfections up to $L/400$ the column span $L$, see [13,15]. Calibrated $\alpha_{imp}$, $\alpha_0$ values have been also proposed for glass panels under various loading and boundary conditions, following the same standardized design approach (see [53–55]). The mentioned formulations, however, are currently intended for single (monolithic or laminated) glass elements only. In addition, given the reference system of Fig. 1(b)–(d), Eq. (1) can provide reliable estimations as far as compressive loads only are applied (i.e. glass self weight and/or additional permanent/accidental loads deriving from the main structure).

### 2.2. Glass members under combined in-plane compression and bending

In most of the cases of practical interest, design pressures acting on the glass surface should be also properly accounted, since potentially responsible of premature collapse mechanisms.

General buckling design rules of design standards for steel members under in-plane compression ($N_{Ed}$) and bending ($M_{Ed}$) could be accounted and adapted for glass systems. According to [56], given a structural element with end-restraints preventing torsional deformations ($W$ the elastic sectional modulus), its buckling resistant domain should be defined so to satisfy the condition:

$$\frac{N_{Ed}}{\chi \cdot \frac{\sigma_R}{\gamma_{M1}} \cdot A} + \frac{M_{Ed}}{\frac{\sigma_R}{\gamma_{M1}} \cdot W \cdot \left(1 - \frac{N_{Ed}}{N_{cr}^{(E)}}\right)} \leqslant 1. \tag{5}$$

While Eq. (5) is primarily intended for single members, careful attention should be spent for IGUs, whose structural performance is affected by the 'coupled' bending response of multiple glass layers (see Sections 3–5).

## 3. Finite element numerical modelling of IGUs

### 3.1. General Finite Element working assumptions

A first set of FE simulations was carried out in ABAQUS [11] on numerical models able to account for the gas cavity effects between the glass layers, for IGUs according to Fig. 1(b)–(d). Due to the high

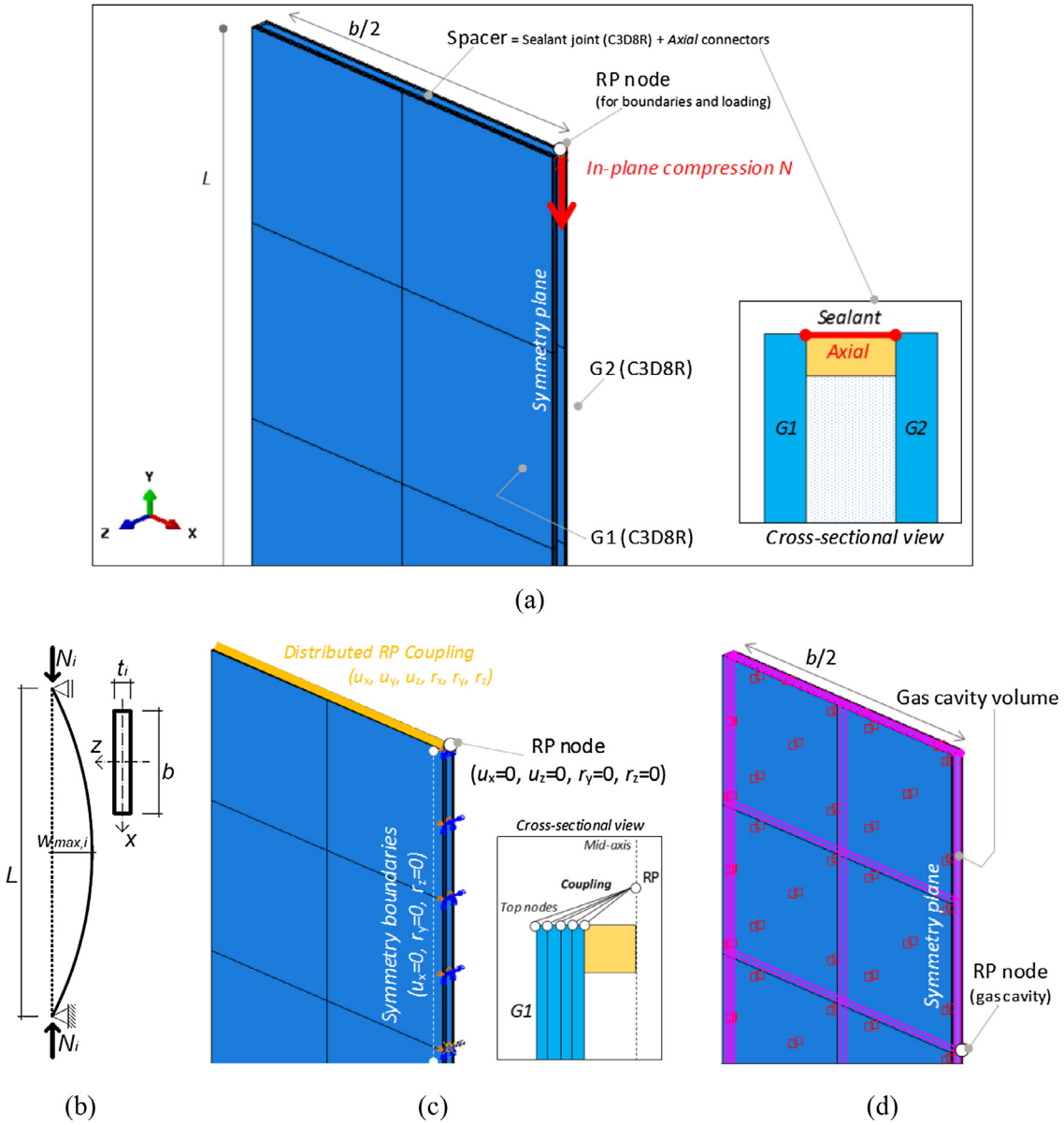


**Fig. 3.** Reference numerical model for the buckling analysis of 2-side supported IGUs (ABAQUS, mesh hidden from view). (a) Assembly and loading, with (b) reference mechanical model and details of (c) boundaries or (d) fluid cavity gap.

sensitivity of typically slender glass panels to out-of-plane deformations, their in-plane compressive buckling response was first investigated, neglecting possible external/internal pressures.

Given two monolithic glass layers, several geometrical configurations of practical interest were explored, including IGUs with different aspect ratios ($\alpha = L/b$, with $L > b$, see Fig. 1(c)), glass thicknesses ($t_1$, $t_2$), gas cavity thickness ($s$), imperfection amplitudes ($w_{0,tot}$). The reference IGU was simply supported along the top/bottom edges, with vertical edges fully unrestrained, see Fig. 1(c). Possible rotational restraints due to supporting devices (see Fig. 1(d)) were fully disregarded.

### 3.2. FE model assembly

The typical FE model consisted of solid brick elements representative of glass panels (C3D8R element types from ABAQUS library [5]). Mesh size and pattern were set in the form of 8-node regular scheme, with 4 elements in the thickness of each glass layer. Given a double IGU, only half geometry was numerically described with symmetry boundary conditions (see Fig. 3(a)).

A set of master 'RP' nodes was defined, for loads, boundaries and interactions (Fig. 3(a)–(d)). On the top/bottom IGU surfaces, two RP nodes were created to assign linear supports and in-plane compressive loads, hence reproducing the mechanical system of Fig. 3(b). The structural interaction between the IGU and each RP node was established in the form of kinematic *coupling* constraints able to restrain relative displacements/rotations of the involved nodes (see Fig. 3(c)).

In terms of mechanical properties of glass, a linear elastic material was defined, with $E_g = 70$GPa, $\nu_g = 0.23$ the nominal modulus of elasticity and Poisson' ratio [52]. Through the incremental simulations reported in the paper, the distribution of maximum tensile stresses $\sigma_{max,i}$ in each glass panel was hence continuously monitored, and compared with the nominal resistance ($\sigma_R = 45$ MPa for annealed glass [52], as in the examples here discussed).

A key role was given to the description of fluid cavity effects. Following Fig. 2, the presence of continuous sealant spacers was accounted in the form of a silicon layer (C3D8R solid brick elements) and a set of mechanical connectors ("*axial*" type of ABAQUS library) able to reproduce a continuous rigid frame along the panels' edges (see

Figs. 2 and 3(a)). For the silicon layer (10 mm × $s$ its cross-sectional dimensions), an equivalent elasto-plastic material was considered ($E_s$ = 3MPa, $\nu_s$ = 0.3 and $\sigma_{s,y} = \sigma_{s,u}$ = 0.15 MPa [57,58]). For the *axial* connectors, fully rigid compressive stiffness/resistance features were taken into account. Special care was indeed spent for their tensile mechanical behaviour, via a brittle elastic constitutive law. In this manner, the possible separation of glass panels' edges due to progressive tensile damage of spacers was taken into account during the out-of-plane deformations of the examined IGUs. Unrealistic deformed shapes were prevented especially along the unrestrained vertical edges of glass panels. Major numerical benefits due to the so defined *axial* connectors were in fact observed through the post-processing phase, close to mid-span sections of vertical edges, due to the attainment of large deformations and a combination of multiple effects deriving from possible combined design loads, gas cavity variations, different flexibility of glass panes, etc. In accordance with Fig. 3(d), finally, the possible transmission of loads from one glass panel to the other (i.e. *load sharing effects* – see also Section 5) was considered via the gas cavity. Following [59], a mechanical "*fluid cavity interaction*" was used (with $M_{air}$ = 28.97 kg/kmol and $p_{air}$ = 1atm the molecular weight and atmospheric pressure). To this aim, a further master RP node representative of the infill features was described at the center of the cavity volume (see Fig. 3(d)).

### 3.3. Solving approach for IGUs under in-plane compression

For each FE model, the typical buckling analysis consisted in two sub-steps.

First, (i) an eigenvalue modal simulation was carried out, so to numerically derive the Euler's critical load and the corresponding buckling shape. The same geometry was used as initial deformation for the second sub-step, namely consisting of (ii) a non-linear geometrical, static incremental analysis. In accordance with [12], each IGU was in fact subjected to an initial global imperfection derived from its fundamental buckling shape, with $w_{0,tot} = L/400$ the mid-span amplitude. The geometrically deformed IGUs were then subjected to linear increasing, compressive loads $N$ acting on the panel top face.

### 3.4. Discussion of FE results

Preliminary FE results were used to assess the theoretical buckling resistance $N_{cr}^{(E)}$ of 2-side supported IGUs in compression, and the accuracy of the standardized curve recalled in Section 2.1 (Eq. (2)), see Fig. 4.

In terms of actual Euler's critical load, the FE investigations emphasized a rather negligible gas cavity structural effect, on the obtained $N_{cr}^{(E)}$ values. A mostly independent bending performance was observed for the glass panels, as in the case of double laminated sections with weak mechanical connection [13]. In other words, simplified but accurate estimations for $N_{cr}^{(E)}$ could be obtained as:

$$N_{cr}^{(E)} = \frac{\pi^2 EI_{abs}}{L^2} \tag{6}$$

where

$$EI_{abs} = \frac{Eb(t_1^3 + t_2^3)}{12}. \tag{7}$$

is the equivalent IGU bending stiffness, see Fig. 4(a).

In Fig. 4(a), a rather close agreement can be perceived for the collected results, where FE dots refer to IGUs with $L$ = 3, 3.5, 4 m, $b$ = 1, 1.5, 2 m, $s$ = 12, 18, 24 mm, and multiple combinations of glass thicknesses $t_1$, $t_2$ (with $t_i$ = 6–20 mm). Following the $N_{cr}^{(E)}$ estimations given by Eq. (6), it is hence expected that the IGU buckling verification could be carried out by means Eqs.(1)–(4), with $\alpha_{imp}$ = 0.6 and $\alpha_0$ = 0.71 (see Section 2.1 and [13]), even neglecting the gas cavity contributions. The FE simulations, in this regard, emphasized a fundamental buckling shape for the examined IGUs in close correlation with a simply supported member in compression, also in presence of different $t_1 \neq t_2$ thicknesses, see the example of Fig. 4(b) – $t_1$ = 15 mm, $t_2$ = 10 mm, $b$ = 2 m, $L$ = 3.5 m.

As far as $N_{cr}^{(E)}$ represents a poor information only, however, further FE assessment of the IGUs compressive performance was carried out by means of static incremental simulations, including comparisons with the standardized curve of Eq. (2). Rather close correlation was observed between analytical and FE predictions ($w_{0,tot} = L/400$, $b$ = 2 m, $L$ = 3.5 m, $s$ = 24 mm and various combinations of $t_1$-$t_2$ thicknesses), see Fig. 4(c). In the figure, labels in brackets are used to give evidence of the FE $t_1$–$t_2$ values, while red numbers denote the first panel expected to crack, under the imposed compressive load $N$.

The collapse load $N_u$ for each "weakest" glass layer was in fact separately collected, so that the numerical coefficient $\chi_{FE}$ could be estimated as:

$$\chi_{FE} = \chi = \frac{N_u}{N_R}, \tag{8}$$

with $N_R = A_{tot} \times \sigma_R = (A_1 + A_2) \times \sigma_R$ the IGU total tensile resistance. Accordingly, the corresponding slenderness was calculated by means of Eq. (4), with $N_{cr}^{(E)} = (N_{cr}^{(E)})_{FE}$.

From Fig. 4(c), it is first possible to perceive the typical high slenderness ratio of IGU geometries. The same results also emphasize the limited IGUs load bearing capacity, with buckling reduction factors in the range of 0.05–0.1. Moreover, the rather good agreement between FE predictions and the standardized curve of Eq. (2) confirms the accuracy of the analytical approach, as far as the examined loading/boundary condition is predominant for the IGUs to verify.

From Fig. 4(c), finally, the actual 'coupled' response of IGU layers can be also perceived (when $t_1 \neq t_2$). Apparently, while Fig. 4(a) highlights that the gas cavity does not affect the $N_{cr}^{(E)}$ value of a given IGU geometry, a certain effect on the glass panels' behaviour can be indeed observed in Fig. 4(c), with the thickest glass layer sustaining the weakest one and leading to a partial increase/decrease of the corresponding resistance. In other words, the single IGU layers cannot be analyzed as fully independent members (Section 2), but require specific methods to account for the composite assembly they belong.

### 3.5. General buckling performance observations and analytical investigation

In order to account for load sharing effects in IGUs in compression, the actual load bearing performance of each glass layer could be rationally derived from Eqs. (6), (7), that is:

$$N_{cr,eff,i}^{(E)} = \frac{A_i}{A_{tot}} N_{cr}^{(E)} = R_{A,i} N_{cr}^{(E)} \quad i = 1,2 \tag{9}$$

Assuming that a single layer sustains part of the total compressive load $N$ (with $R_{A,i}$ = 0.5 for the limit, symmetrical condition $t_1 = t_2$), the corresponding load–displacement response can be in fact estimated via an equivalent thickness $t_{eff,i}$ given by:

$$t_{eff,i} = \sqrt[3]{\frac{12 I_{eff,i}}{b}}, \tag{10}$$

with:

$$I_{eff,i} = \frac{N_{cr,eff,i}^{(E)} L^2}{\pi^2 E} \tag{11}$$

As a result, pre-design considerations for IGUs in compression could be obtained from simple analytical estimations, leading to optimal combinations of glass thicknesses. In the current design practice, IGUs are in fact generally obtained by assembling different thicknesses, due to thermal and safety motivations, hence resulting in un-symmetrycal composite sections.

Given an IGU with $t_1 > t_2$, it is hence expected from Eq. (9) that:

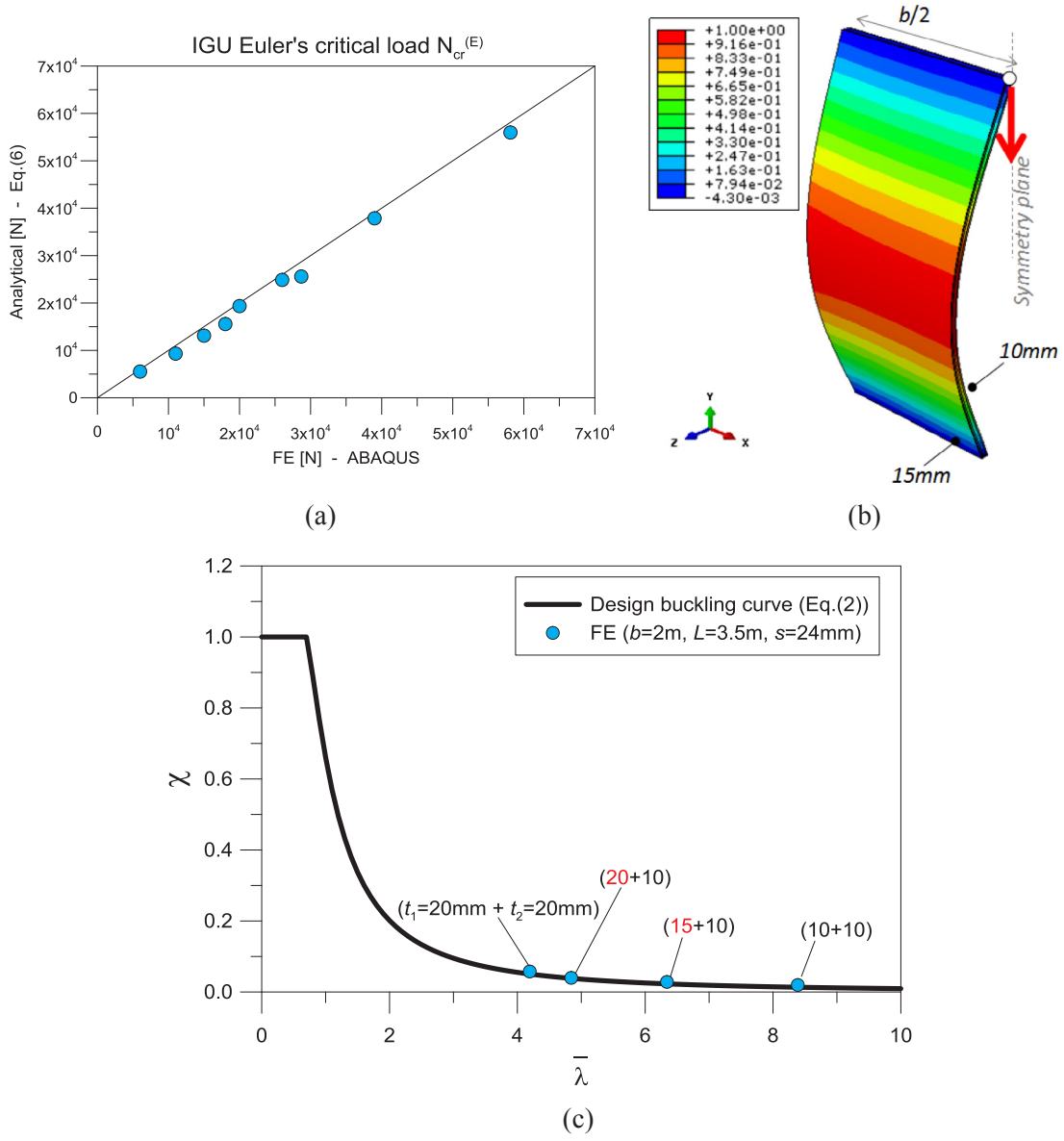


**Fig. 4.** Buckling performance assessment of IGUs in compression. (a) Analytical and numerical comparisons of Euler's critical loads, with (b) typical buckling shape. (c) Numerical validation of the standardized curve for single glass members (Eq. (2)).

– the total Euler's critical load $N_{cr}^{(E)}$ of the IGU is given by Eq. (6):
– $t_{eff,1} < t_1$, that is:

$$N_{cr,eff,1}^{(E)} = \frac{\pi^2 EI_{eff,1}}{L^2} < N_{cr,1}^{(E)} = \frac{\pi^2 EI_1}{L^2} \tag{12a}$$

– $t_{eff,2} > t_2$, hence:

$$N_{cr,eff,2}^{(E)} = \frac{\pi^2 EI_{eff,2}}{L^2} > N_{cr,2}^{(E)} = \frac{\pi^2 EI_2}{L^2}; \tag{12b}$$

Given the $i$-th glass pane under $N_i$ compressive load (Eq. (9)), moreover, its bucking analysis should account for possible geometrical imperfections $w_{0,tot}$. The actual load-displacement response of each glass layer, in this sense, could be predicted as [13]:

$$w_{eff,i} = w_{0,tot}\left(\frac{1}{1-N_i/N_{cr,eff,i}^{(E)}}\right) \tag{13}$$

with maximum stresses given by [13]:

$$\sigma_{max,i} = -\frac{N_i}{A_i} + \frac{N_i w_{eff,i}}{W_i}, \tag{14}$$

and $W_i = bt_i^2/6$.

In order to validate the here proposed analytical approach for IGUs, comparative calculations are collected in Fig. 5(a), as obtained from Eqs. (13), (14) and FE simulations. The case study reported in Fig. 5(a) is an IGU with $t_1 = 20$ mm, $t_2 = 10$ mm, $b = 1$ m, $L = 3$ m ($s = 24$ mm). Given the theoretical IGU resistance $N_{cr}^{(E)} = 57.6$ kN (see Eq. (11)), the single glass layers are expected to offer – as independent layers – an ideal critical load equal to $N_{cr,1}^{(E)} = 51.2$ kN and $N_{cr,2}^{(E)} = 6.4$ kN, respectively (i.e. the asymptotic value of load-displacement curves [13]). Based on Eqs. (12a), (12b), however, the 'coupled' buckling response of the same panels can be described via the effective IGU thicknesses given by Eq. (10), that is $t_{eff,1} = 18.1$ mm and $t_{eff,2} = 14.4$ mm, hence leading to marked variations in the corresponding load-displacement responses.

For the $t_1$ and $t_2$ independent panels, it can be shown that the proposed load-displacement curves tend asymptotically to their critical loads $N_{cr,1}^{(E)}$ and $N_{cr,2}^{(E)}$. However, most of the total compression is sustained by the thickest layer ($t_2$) and its mechanical response is

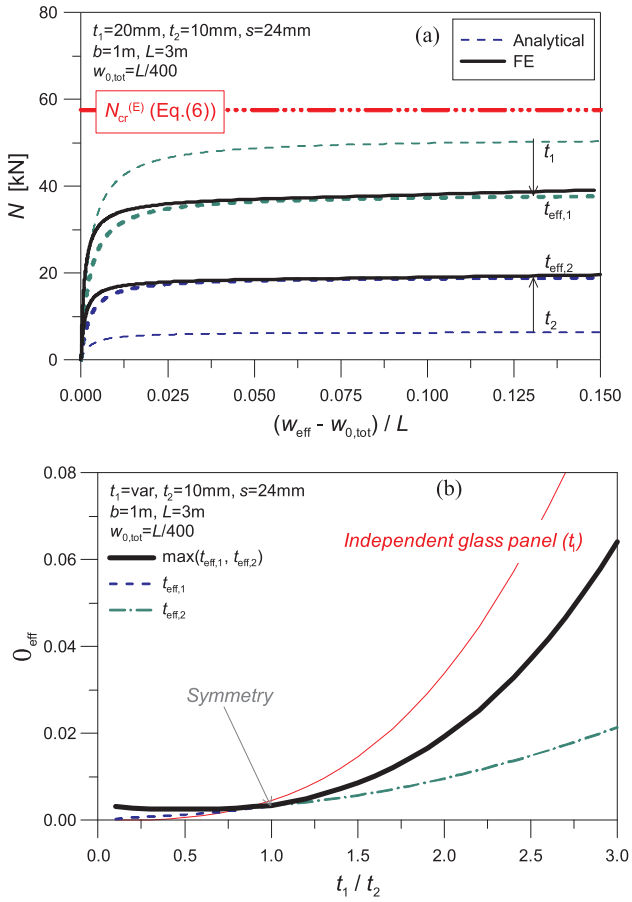


**Fig. 5.** Effect of thickness variations on the buckling response of IGUs in compression. Analytical (Eq. (13)) and numerical (ABAQUS) load-displacement response of IGU layers ($t_{eff,1}$ and $t_{eff,2}$), compared to independent $t_1$ and $t_2$ panels; (b) expected buckling reduction coefficient $\chi_{eff}$ for $t_{eff,1}$ and $t_{eff,2}$ glass layers (Eq. (8)), by varying $t_1$.

affected by the adjacent panel ($t_2 < t_{eff,2}$), that conversely takes advantage from the first one ($t_{eff,1} < t_1$). As such, the 'effective' theoretical resistance values are $N_{cr,eff,1}^{(E)} = 38.38\,kN < N_{cr,1}^{(E)}$ and $N_{cr,eff,2}^{(E)} = 19.19\,kN > N_{cr,2}^{(E)}$ (see Eqs. (12a), (12b), or the asymptotic values of $t_{eff,1}$ and $t_{eff,2}$ curves in Fig. 5(a)).

In other words, the buckling analysis of $t_1$–$t_2$ 'independent' glass panels would lead to poor and non-conservative predictions for their actual load bearing capacity, as a part of an IGU, with up to 25% the scatter in the actual Euler's loads. In Fig. 5(a), the close correlation between analytical and numerical estimations for effective glass thicknesses can be also noticed, hence suggesting the accuracy of the simplified analytical assumptions here discussed.

Practical qualitative findings are also emphasized in Fig. 5(b), where the same IGU of Fig. 5(a) is investigated. There, the $t_1$ thickness is parametrically modified, in the range from 1 mm to $3 \times t_2 = 30$ mm (with $t_2 = 10$ mm, $b = 1$ m, $L = 3$ m, $s = 24$ mm). Analytical results are obtained from Eqs. (13), (14), then normalized via Eq.(8) and proposed as a function of the $t_1/t_2$ ratio, in the form of an 'effective' buckling reduction coefficient $\chi_{eff}$ for each glass layer. The maximum envelope of analytical data is also emphasized (see the "max($t_{eff,1}$, $t_{eff,2}$)" curve), being representative of the actual reduction coefficient for the full IGU. The red curve, finally, represents the $\chi$ reduction factor analytically derived for an 'independent' thickness $t_1$, by fully disregarding the fluid cavity interaction effects with the adjacent panel.

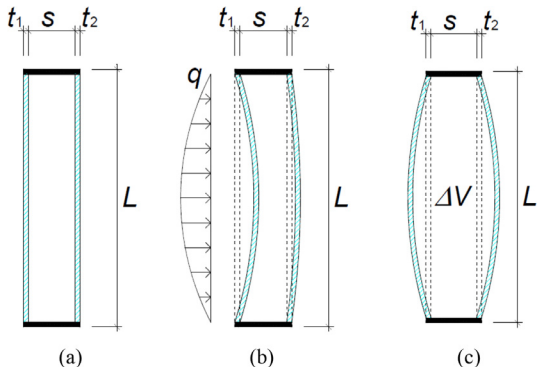


**Fig. 6.** Cavity volume variations in an IGU system (a) due to possible (b) external or (c) internal (environmental) pressures, in accordance with [45].

## 4. IGUs under combined compression and bending

Following Section 3, further IGU configurations were numerically investigated under the effects of combined compressive/bending loads, so to assess the *load sharing effects* on their overall stability, see Fig. 6 and [45].

### 4.1. Discussion of FE methods, results and reference analytical models

Given an IGU system according to Section 3, FE simulations consisting of three sub-steps were carried out, including:

(i) an eigenvalue analysis for the IGU in compression (to estimate its Euler's critical load and fundamental buckling shape), and
(ii) a static incremental simulation, consisting of two loading stages (ii-A, ii-B) and inclusive of an initial global imperfection ($w_{0,tot} = L/400$)

In accordance with Fig. 6(b) and (c), the effects of both external pressures $q$ or environmental loads were separately assessed. As such, the reference incremental simulation included:

(ii-A) the application of an external distributed pressure $q$ according to Fig. 6(b) – (or a temperature gradient within the cavity),
(ii-B) and a subsequent, linear increasing compressive load $N$.

Parametric FE estimations were hence assessed towards analytical methods of literature, see Sections 4.1.1 and 4.1.2.

#### 4.1.1. External pressures

Globally, the assigned pressures $q$ manifested in the form of additional initial imperfections for the examined IGUs, that is in a deformed shape still in accordance with Fig. 4(b), but in a further marked increase of bending deformations/stress peaks. Such an outcome is in close correlation with the analytical findings reported in [13] for 'independent' glass members. As shown in Fig. 7(b), as far as the amplitude of $q$ pressures increases, large out-of-plane deformations are first attained, for a given geometry. A direct effect is a reduction of the global load bearing capacity, due to premature tensile stress peaks. Such an effect, however, cannot be perceived from Euler's critical load values only.

To this aim, further FE incremental results are reported in Fig. 7(c), to assess the accuracy of Eq. (5) when applied to composite IGU sections. In particular, Fig. 7(c) is representative of the ($N$, $M$) resisting domain for the full IGU to verify, being affected by the tensile failure of the weakest glass layer. FE data are proposed for an IGU with $b = 2$ m, $L = 3$, $t_1 = 20$ mm, $t_2 = 10$ mm ($s = 24$ mm). The 'collapse' configuration for a general ($N$, $M$) combination of loads was detected as the first $\sigma_{max,i} = \sigma_R$ attainment in glass layers, by monitoring the stress

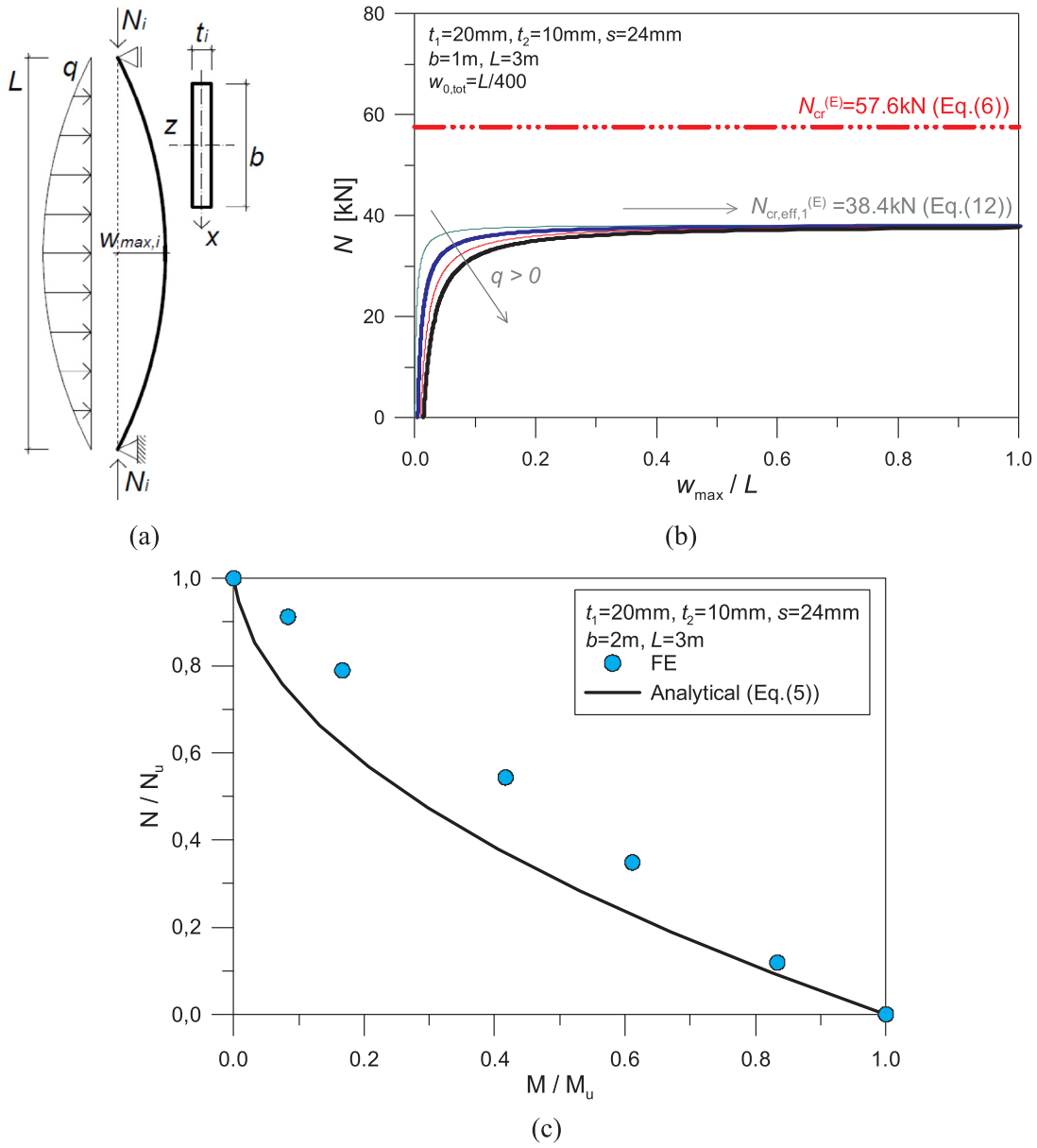


**Fig. 7.** IGUs under combined compression/bending (examples referred to external pressures $q$). (a) reference analytical model, with (b) $q$ effects on the load-displacement response of $t_1$ IGU panel and (c) numerical derivation of the ($N$, $M$) resisting domain.

evolution. Given an assigned pressure $q$, the corresponding bending moment was estimated as $M_{max} = M_u = qL^2/8$, while linearly increasing the compressive load $N$ up to the first tensile failure. Taking advantage of FE modelling assumptions summarized in Section 3, the total compressive load $N$ was taken up in the ratio $N_i$ (Eq. (9)) by each glass layer. The external pressure $q$ was indeed shared between the two glass panels, thanks to the gas cavity.

The limit $N = 0$ and $M = 0$ conditions were first numerically investigated, including additional normalized FE results for various ($N$, $M$) configurations. The so collected ultimate ($N_u$, $M_u$) numerical dots were then normalized in accordance with Eq. (5), with $\gamma_{M1} = 1$, $\sigma_R = 45$ MPa, $\chi$ and $N_{cr}^{(E)}$ given by Eqs. (2) and (6) respectively. According to Eq. (5), careful consideration was finally spent for the analytical estimation of the IGU sectional modulus $W$. Rationally, this term was analytically derived by accounting for the conventional bending resistance definition, as well as for the IGU intrinsic features (i.e. composite section with weak mechanical connection between the glass layers, see also Eq. (7)), that is:

$$M_R = \sigma_R \cdot W_{abs} = \sigma_R \cdot \frac{b}{6}\left(t_1^2 + \frac{t_1}{t_2}t_2^2\right), \quad (\text{with } t_1 > t_2) \tag{15}$$

hence leading to $M_R = 9$ kNm, with $W_{abs} = 2 \times 10^5$ mm$^3$ denoting the IGU elastic sectional modulus for the reported case study.

For all the FE dots in Fig. 7(c), the thickest layer ($t_1 = 20$ mm) was generally observed to first attain the tensile resistance of glass, hence representing the IGU weakest component.

A good correlation was found between FE and analytical results of Fig. 7(c), and mainly for the limit compressive/bending conditions.

In the ($M = 0$) limit case, a FE collapse load $N_u = 106.45$ kN tending to $N_{cr}^{(E)} = 115.15$ kN (Eq. (6)) was predicted, with $N_{cr,eff,1}^{(E)} = 76.76$ kN and $N_{cr,eff,2}^{(E)} = 38.38$ kN respectively ($R_{A,1} = 0.66$ and $t_{eff,1} = 18.17$ mm, that is $\approx 0.9 \times t_1$). The tensile resistance of annealed glass was first attained in the $t_1$ panel, for $N_{u,1} = R_{A,1} \times N_u = 70.9$ kN (with $\sigma_{max,2} = 40$ MPa in the $t_2$ layer). The analytical calculations from Eqs. (13), (14) suggested a first cracking occurrence in the $t_1$ panel, at $N_{u,1} = 70.28$ kN (with $N_u = 105.52$ kN), hence resulting in close correlation with the FE predictions. Given the

analytical $N_{u,1}$ value, a maximum stress of $\sigma_{max,2} = 38$ MPa was calculated in the $t_2$ layer, in accordance with FE observations.

For the same IGU in bending ($N = 0$), a total ultimate moment $M_u \approx 8.5$ kNm was numerically calculated (with $q_u = 7.56$ kN/m$^2$ the corresponding pressure, see Fig. 7(c)), hence in close agreement with Eq. (15).

In conclusion, given a general ($N$, $M$) configuration, Eq. (5) proved to represent a conservative and practical resisting domain for the examined IGU, hence offering a suitable tool for design. The simplified assumptions of Eq. (5), see Fig. 7(c), typically resulted in an upward concavity of the ($N$, $M$) domain, leading to safe predictions for mostly linear ($N$, $M$) non-dimensional FE estimations.

Given the general FE observations partly discussed in this paper, simplified analytical models should be assessed for practical use in design. Under a ($N$, $M$) loading condition, the structural performance of a 2-side supported IGU could be rationally referred to Fig. 7(a) and properly described via a combination of analytical methods in use for single glass members and IGUs in put-of-plane bending (see [12,13,15,45]). According to Fig. 7(a), each $t_i$ panel is in fact expected to sustain a $N_i$ ratio of the total compression $N$ (see Eq. (9)) and part ($q_i$) of the assigned pressure, due to lad sharing effects. Given a $q$ amplitude, its overall effects are conventionally assumed to share between the IGU glass plies, as recalled in Appendix A [45].

Following [13] – once the $t_{eff,i}$ thicknesses and the $N_i$, $q_i$ loading terms are calculated via Eqs. (9), (10) and Appendix A – the load-stress response of each IGU glass layer can be assessed as a function of its effective deformation:

$$w_{eff,i} = \frac{L^2(q_i L^2 + 8N_i w_{0,tot})}{8(EI_{eff,i}\pi^2 - N_i L^2)} \tag{16}$$

and maximum stresses in glass:

$$\sigma_{max,i} = -\frac{N_i}{A_i} \pm \frac{N_i w_{eff,i}}{W_i} \pm \frac{q_i L^2}{8W_i} \tag{17}$$

Fig. 8 presents a selection of analytical calculations, giving evidence of the marked reduction in the expected compressive buckling resistance for an IGU under ($N$, $M$) loads. The maximum stresses $\sigma_{max,i}$ in each panel are estimated following Eqs. (16), (17) and Appendix A. The corresponding reduction coefficient $\chi_{eff}$ is still derived from Eq. (8), while comparative results are proposed as a function of the geometrical slenderness:

$$\lambda = \frac{L}{\rho} = \frac{L}{\sqrt{\frac{I_{abs}}{A_1 + A_2}}}, \tag{18}$$

with $I_{abs}$ given by Eq. (7).

For the examined geometrical configurations, the cavity thickness $s$ has negligible effects, compared to the marked reduction of buckling resistance due to external pressures $q$, see Fig. 8(a) and (b). In the same figures, additional FE dots are proposed, giving evidence of the close correlation between numerical predictions and simplified analytical estimations.

#### 4.1.2. Temperature gradients

Finally, the effects of additional environmental loads were separately assessed, in accordance with the FE approach of Section 4.1.

Given a set of IGU geometries and the reference production temperature $T_P = 20$ °C, a temperature gradient $\Delta T > 0$ was imposed to the air infill of the cavity. In accordance with Fig. 6(c), such an increase of temperature typically manifested in a cavity volume increase, hence in further imperfections to account with the assigned initial deformations $w_{0,tot}$.

In this context, while the initial geometrical imperfections were assumed to have the same direction for both the glass plies (i.e. Fig. 4(b)), both safe and unsafe effects were observed due to the cavity volume increase.

Following Eqs. (16), (17) and [45], possible environmental phenomena inclusive of temperature ($\Delta T$, in [K]), pressure ($\Delta p$, in [atm]) and altitude ($\Delta h$, in [m]) variations should be in fact considered in the form of an internal pressure $q_i = \pm \varphi p_0$ acting on both the glass layers, with $\varphi$ given in Appendix A and:

$$p_0 = p_{h,0} + p_{C,0} = c_h \cdot \Delta h + c_T \cdot \Delta T, \tag{19}$$

where $c_h = 0.012$ kPa/m and $c_T = 0.34$ kPa/K.

In this regard, Fig. 9(a) presents non-dimensional analytical and FE results ($\Delta T > 0$, $T_P = 20$ °C) for an IGU with $t_1 = t_2 = 10$ mm, $b = 1$ m, $L$ variable, $s = 24$ mm, $w_{0,tot} = L/400$. As shown, rather close correlation can be generally observed between the collected data. The major outcome of Fig. 9(a), however, is represented by the marked reduction of the actual $\chi_{eff}$ coefficient for the examined IGU, as far as $\Delta T$ increases. Environmental phenomena should be properly considered, especially when a combination of multiple design actions and/or imperfections or eccentricities is expected during the life time of a given IGU. As proposed in Fig. 9(a), for slender IGUs ($\lambda > 500$, in the proposed case study) the theoretical buckling resistance could in fact also vanish (i.e. $\chi_{eff} \to 0$) due to temperature variations, hence requiring careful consideration at the design stage.

In Fig. 9(b) and (c), temperature gradients effects are further reported in combination with IGU geometrical variations, like the initial imperfection amplitude ($w_{0,tot}$) or the cavity thickness ($s$). There, the IGUs high susceptibility to possible stability losses is again emphasized, suggesting the use of specific methods for their analysis and verification.

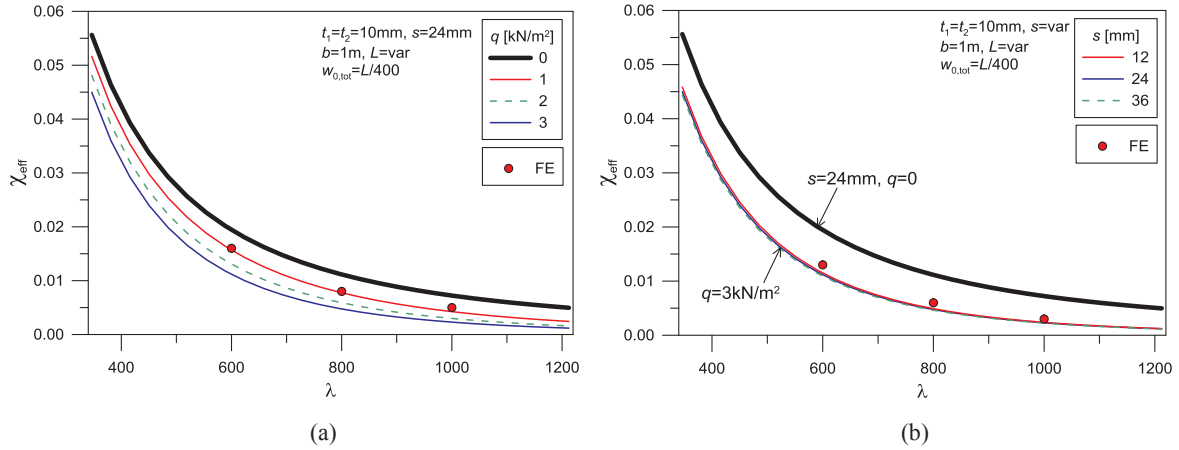


**Fig. 8.** Effect of external pressures $q$ on the buckling resistance of a given IGU in compression, including variations in: (a) $q$ amplitude or (b) cavity thickness.

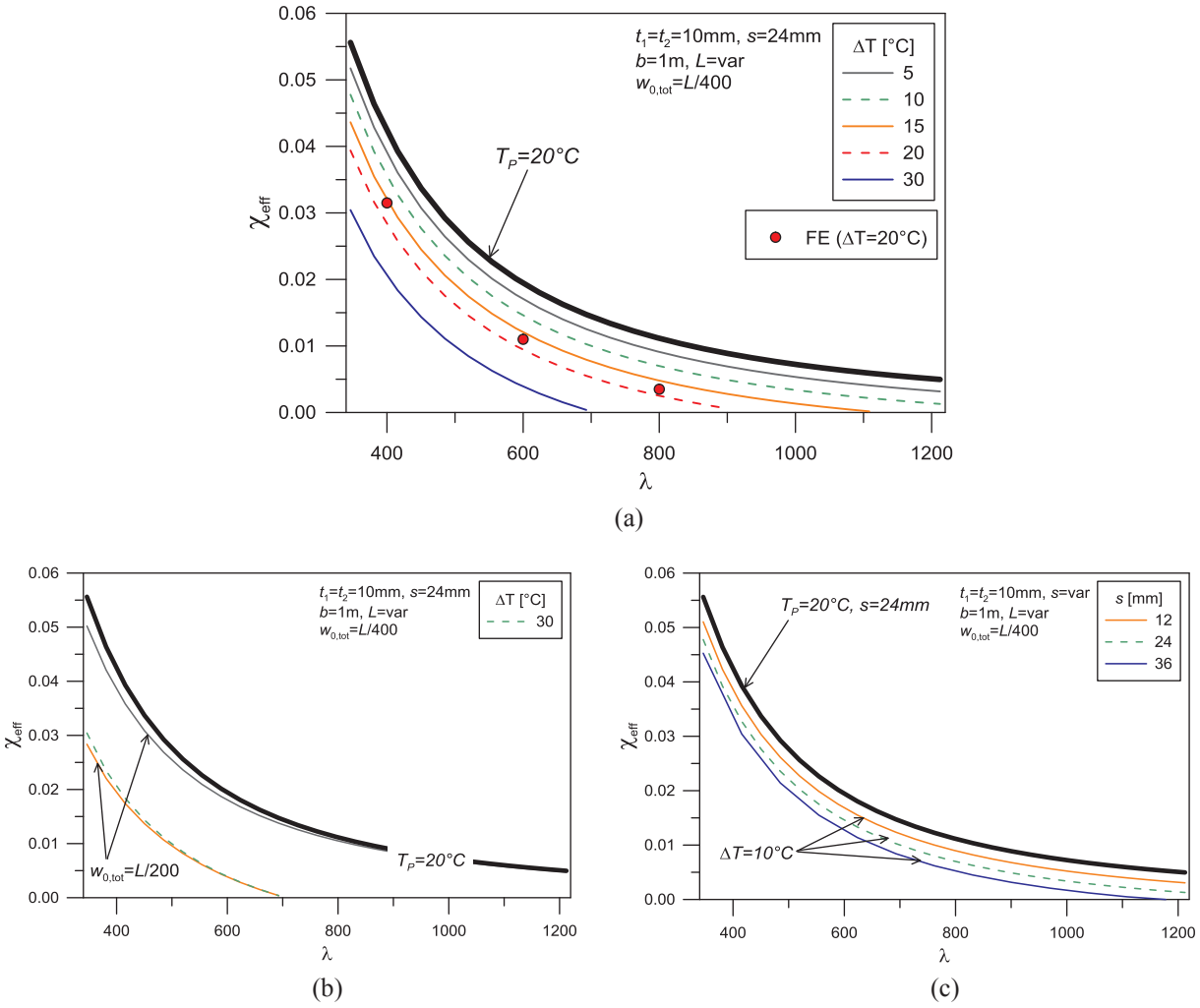


**Fig. 9.** Effect of environmental loads on the buckling resistance of a given IGU in compression, including variations in: (a) temperature; (b) initial imperfection or (c) cavity thickness.

## 5. Conclusions

In this paper, the buckling performance of IGUs in use for facades and envelopes was investigated via Finite Element (FE) numerical and analytical models.

Special care, in accordance with recent design trends and the typically high buckling vulnerability of glass systems, was spent for 2-side supported IGUs, with top/bottom continuous restraints and vertical edges unrestrained.

Differing from single glass members – whose buckling analysis can be rationally carried out under several boundary/loading conditions, based on analytical formulations and standardized approaches of literature – the buckling performance of IGUs should be properly assessed. IGUs are in fact characterized by additional *load sharing* effects, hence requiring specific studies and design methods.

To this aim, refined FE models were first presented in the paper, to emphasize the actual load bearing performance of the IGUs in compression by accounting for gas cavity effects. The FE simulations partly discussed in the paper generally highlighted that:

- simplified analytical methods can accurately estimate the Euler's critical load of 2-side supported IGUs
- the fundamental buckling shape is in close correlation with simply supported composite columns, hence revealing mostly negligible structural effects due to the gas cavity
- the actual load bearing capacity and compressive buckling resistance of IGUs is limited, due to high slenderness ratios and sensitivity to geometrical imperfections and glass thicknesses
- due to the gas cavity infill, accurate load-displacement analytical calculations and buckling estimations can be obtained as far as "effective" glass thicknesses are accounted, as in the case of composite sections with weak connection. The analysis of single 'independent' glass members would result in unsafe predictions (with up to 25% the scatter for the reported case studies)

Subsequently, the IGUs buckling performance under combined compression/bending ($N$, $M$) was also explored, including both external pressures and internal (environmental) loads. The additional bending loads generally proved to have marked effects on the observed buckling responses, since leading to premature large deflections and collapse. A suitable tool for buckling purposes was found in the conventional ($N$, $M$) domain in use for single structural members, with careful consideration for IGUs features. Simplified analytical models proved to offer reliable predictions, compared to advanced FE estimations. In conclusion, both the FE and analytical studies highlighted the high sensitivity of the examined IGUs to even moderate temperature variations, requiring careful consideration at the design stage.

**Table 1**
Load sharing approach for IGUs under external pressures $q$, in accordance with [45].

| Loaded panel | Load sharing effect | |
|---|---|---|
| | $t_1$ | $t_2$ |
| $t_1$ (outside) | $q_1 = (k_1 + \varphi k_2)q$ | $q_2 = (1-\varphi)k_2 q$ |
| $t_2$ (inside) | $q_1 = (1-\varphi)k_1 q$ | $q_2 = (\varphi k_1 + k_2)q$ |

## Appendix A

Key parameters for the calculation of load sharing effects in IGU panels (see Table 1):

$$k_1 = \frac{t_1^3}{t_1^3 + t_2^3}, \tag{A1}$$

$$k_2 = 1-k_1, \tag{A2}$$

$$\phi = \frac{1}{1 + \left(\frac{a}{a^*}\right)^4}, \tag{A3}$$

$$a^* = 28.9\sqrt[4]{\frac{t_1^3 t_2^3 s}{(t_1^3 + t_2^3)k_5}}, \tag{A4}$$

with $a = \min(L,b)$ and $k_5$ given in [45] as a function of the IGU aspect ratio.

## References


[1] Haldimann M, Luible A, Overend M. Structural use of glass. IABSE; 2008. ISBN 978-3-85748-119-2.
[2] Feldmann M, Kasper R, Abeln B, Cruz P, Belis J, Beyer J, et al. Guidance for European Structural design of glass components – support to the implementation, harmonization and further development of the Eurocodes. Report EUR 26439, Joint Research Centre-Institute for the Protection and Security of the Citizen; 2014. http://dx.doi.org/10.2788/5523, Pinto Dimova, Denton Feldmann (Eds.).
[3] Van Den Bergh S, Hart R, Petter Jelle B, Gustavsen A. Window spacers and edge seals in insulating glass units: a state-of-the-art review and future perspectives. Energy Build 2013;58:263–80.
[4] Wüest T, Luible A. Increased thermal induced climatic load in insulated glass units. J Facade Des Eng 2016;4:91–113.
[5] Zajas J, Heiselberg P. Parametric study and multi objective optimization of window frame geometry. Build Simul 2014;7(6):579–93.
[6] Pascual C, Montali J, Overend M. Adhesively-bonded GFRP-glass sandwich components for structurally efficient glazing applications. Compos Struct 2017;160:560–73.
[7] Bedon C, Pascual C, Luna-Navarro A, Overend M, Favoino F. Thermo-mechanical investigation of novel GFRP-glass sandwich facade components. In: Proceedings of Challenging Glass 6, TU Delft, The Netherlands (USB drive); 2018.
[8] Buildings Department. Code of Practice for Structural Use of Glass 2018; 2018, free download: www.bd.gov.hk/english/documents/coee/SUG2018e.pdf [accessed April 2018].
[9] Mocibob D. Glass panel under shear loading – use of glass envelopes in building stabilization [PhD Dissertation]. Switzerland: École Polytechnique Fédérale de Lausanne (EPFL); 2008 Free download (accessed December 2017): https://infoscience.epfl.ch/record/125889.
[10] Bedon C, Amadio C. Exploratory Finite-Element investigation and assessment of standardized design buckling criteria for two-side linear adhesively supported glass panels under in-plane shear loads. Eng Struct 2016;106:273–87.
[11] ABAQUS® version 6.14, Simulia, Dassault Systemes, RI, USA; 2017.
[12] Bedon C, Amadio C. Design buckling curves for glass columns and beams. Struct Build 2015;168(7):514–26.
[13] Amadio C, Bedon C. Buckling of laminated glass elements in compression. J Struct Eng 2011;137(8):803–10.
[14] Amadio C, Bedon C. Buckling of laminated glass elements in out-of-plane bending. Eng Struct 2010;32(11):3780–8.
[15] CNR-DT/210. Guide for the design, construction and control of structures made of glass structural elements [in Italian]. National Research Council (CNR); 2013.
[16] Luible A. Stabilität von tragelementen aus glass [PhD thesis]. Switzerland: École Polytechnique Fédérale de Lausanne (EPFL); 2004 Free download (accessed December 2017): https://infoscience.epfl.ch/record/33486.
[17] Foraboschi P. Experimental characterization of non-linear behavior of monolithic glass. Int J Non Linear Mech 2014;67:352–70.
[18] van Heugten R, Teuffel P, Lindner G, Nijsse R. Load-bearing glass columns – the stacked column. In: Proceedings of Challenging Glass 4 & COST Action TU0905 Final Conference. Lausanne, Switzerland; 2014. p. 717–724.
[19] Bedon C, Amadio C. Flexural-torsional buckling: experimental analysis of laminated glass elements. Eng Struct 2015;73:85–99.
[20] Jakab A, Nehme K, Nehme SG. Fracture behaviour of glass columns experimental study of axial loaded glass columns. In: IOP Conf. Series: Materials Science and Engineering. vol. 123, article 012056; 2016. http://dx.doi.org/10.1088/1757-899X/123/1/012056.
[21] Pešek O, Horáček M, Melcher J. Experimental verification of the buckling strength of structural glass columns. Procedia Eng 2016;161:556–62.
[22] Liu Q, Huang X, Liu G, Zhou Z, Li G. Investigation on flexural buckling of laminated glass columns under axial compression. Eng Struct 2017;133:14–23.
[23] Bedon C, Kalamar R, Eliášová M. Low velocity impact performance investigation on square hollow glass columns via full-scale experiments and Finite Element analyses. Compos Struct 2018;182:311–25.
[24] Arasteh D, Selkowitz S, Wolfe JR. The design and testing of a highly insulating glazing system for use with conventional window systems. J Sol Energy Eng 1989;111(1):44–53.
[25] Giovannetti F, Kirchner M, Kliem F, Hoeltje T. Development of an insulated glass solar thermal collector. Energy Procedia 2014;48:58–66.
[26] Torok GR, Major AL. Predicting time-to-fogging of Insulating Glass Units. Report (Technical Series 05-117); 2005, free download (accessed December 2017): http://publications.gc.ca/site/eng/391905/publication.html.
[27] Basok BI, Davydenko BV, Isaev SA, Goncharuk SM, Kuzhel' LN. Numerical modeling of heat transfer through a triple pane window. J Eng Phys Thermophys 2016;89(5):1277–83.
[28] Scherer C, Semar E, Becker H, Wittwer W, Wolthaus J, Scherer T. A new reactive thermoplastic spacer with excellent durable energy efficiency for structural glazing facades. In: Proceedings of Challenging Glass 5 Conference, Ghent, Belgium (USB drive); 2016.
[29] Kwapisz L, Maurin A, Jakubowski P. Numerical modelling of sound transmission through the window type partition. Vib Phys Syst 2016;27:211–8.
[30] Okubo H. A study on durability of insulating glass units for frameless glazing systems. In: Proceedings of Glass Processing Days 2003, Tampere, Finland; 2003. www.glassfiles.com.
[31] Chesnokov AG, Chesnokov SA. Some steps in the methods of the IGU characteristics calculation evolution. In: Proceedings of glass processing days 2005, Tampere, Finland; 2005. www.glassfiles.com.
[32] Eekhout M, Weber L, Niderehe S. Transparent cubical glass building in madrid. In: Proceedings of Glass Performance Days 2009, Tampere, Finland; 2009. www.glassfiles.com.
[33] Vollers K, Van den Engel G. Framing systems for façades of non-standard geometry. In: Proceedings of Glass Processing Days 2005, Tampere, Finland; 2005. www.glassfiles.com.
[34] Eekhout M, Van de Rotten P. Development of a Super Slim Façade System for INHolland Polytechnic, Delft. In: Proceedings of Glass Performance Days 2009, Tampere, Finland; 2009. www.glassfiles.com.
[35] Neugebauer J. A design concept for bent insulated glasses for the reading room of the Berlin State Library. In: Proceedings of Glass Performance Days 2009, Tampere, Finland; 2009. www.glassfiles.com.
[36] Giesecke AH, Wolf AT. Structural glazing silicone in gas filled insulating glass – Main Airport Center. In: Proceedings of Glass Processing Days 2005, Tampere, Finland; 2005. www.glassfiles.com.
[37] Shi Y, Sun W, Wang Y, Luo Y, Xu Y. The pressure distribution of insulating glass

units under thermal gradient. In: Proceedings of ICETCE International Conference on Electric Technology and Civil Engineering; 2011. http://dx.doi.org/10.1109/ICETCE.2011.5775852.
[38] Morse SM, Norville HS. Comparison of methods to determine load sharing of insulating glass units for environmental loads. Glass Struct Eng 2016;1(1):315–29.
[39] Buddenberg S, Hof P, Oechsner M. Climate loads in insulating glass units: comparison of theory and experimental results. Glass Struct Eng 2016;1(1):301–13.
[40] Huveners EMP, Van Herwijmen F, Soetens F. Load sharing in insulated double glass units. Heron 2003;48(2):99–122.
[41] Panait A, Cossavella M, Delsahut G, Galéa JL, Morcant K. Insulating glass units: the effects of seal stresses and deformations on durability and service life. In: Proceedings of Glass Performance Days 2007, Tampere, Finland; 2007. www.glassfiles.com.
[42] Feldmeier F. Insulating units exposed to wind and weather – load sharing and internal loads. Proceedings of Glass Processing Days 2003, Tampere, Finland; 2003. www.glassfiles.com.
[43] Iker J, Wolf AT. Secondary stresses induced by shear movement in structural glazing sealants. Mater Struct 1992;25:137–44.
[44] Hagl A. Experimental and numerical analysis of edge seals spacers of insulated glass units for structural sealant glazing applications. In: Proceedings of Challenging Glass 3 Conference; 2012.
[45] prEN 13474-1. Glass in building – design of glass panes – part 1: general basis of design. Brussels, Belgium: CEN – European Committee for Standardization; 2007.
[46] Austrian Standards Institut, ÖNORM B 3716 – Part 1 – glas im Bauwesen; 2006.
[47] Tibolt M, Odenbreit C. The stress peak at the borehole of point-fitted IGU with undercut anchors. J Facade Des Eng 2015;2(1–2):33–66.
[48] Broker KA, Fisher S, Memari AM. Seismic racking test evaluation of silicone used in a four-sided structural sealant glazed curtain wall system. J ASTM Int, STP 1545:473–504. http://dx.doi.org/10.1520/STP154520120023.
[49] Brendler S, Haufe A, Ummenhofer T. A detailed numerical investigation of insulated glass subjected to the standard pendulum test. In: Proceedings of the 3 LS-DYNA FORUM 2004, Bamberg; 2004 www.dynamore.de/download/af04/papers/F-I-5.pdf.
[50] Deng R, Jin X. Numerical simulation for blast analysis of insulating glass in a curtain wall. Int J Comput Methods Eng Sci Mech 2010;11(3):162–71.
[51] Larcher M, Manara G. Influence of air damping on structures especially glass. JRC Technical Notes –PUBSY JRC 57330, European Commission Publications Office; 2010.
[52] EN 572-2. Glass in buildings – basic soda lime silicate glass products. Brussels, Belgium: CEN; 2004.
[53] Bedon C, Belis J, Amadio C. Structural assessment and lateral-torsional buckling design of glass beams restrained by continuous sealant joints. Eng Struct 2015;102:214–29.
[54] Bedon C, Amadio C. A unified approach for the shear buckling design of structural glass walls with non-ideal restraints. Am J Eng Appl Sci 2016;9(1):64–78.
[55] Bedon C, Amadio C. Shear glass panels with point-fixed mechanical connections: Finite-Element numerical investigation and buckling design recommendations. Eng Struct 2016;112:233–44.
[56] EN 1993-1-1. Eurocode 3 – design of steel structures – Part 1–1: general rules and rules for buildings. Brussels, Belgium: CEN; 2005.
[57] Dow Corning. Silicone Structural Glazing Manual, free download [accessed December 2017]: https://www.dowcorning.com/content/publishedlit/62-0979c-01.pdf.
[58] Wolf AT. Silicone sealed insulating glass units. In: Proceedings of ISAAG - International Symposium on the Application of Architectural Glass, Munich, Germany; 2004.
[59] Bedon C, Amadio C. Enhancement of the seismic performance of multi-storey buildings by means of dissipative glazing curtain walls. Eng Struct 2017;152:320–34.